CO_2 Corrosion Inhibitors Performance at Deposit-Covered Carbon Steel and Their Adsorption on Different Deposits

Erika M. Suarez, Laura L. Machuca,* Brian Kinsella,* and Kateřina Lepková‡,**

The efficiency of inhibitors to prevent under deposit corrosion of carbon steel and their adsorption on aluminum oxide, calcium carbonate, and silica sand deposits have been evaluated using electrochemical measurements and UV-visible spectroscopy. 2-Mercaptopyrimidine provided the highest corrosion protection on both bare and deposit-covered steels. In contrast, 1-Dodecylpiridinium chloride had minimal adsorption on all deposits, but it exhibited insufficient performance. Inhibitors adsorption tended to be related to the inhibitor type and not notably to the physical properties of the deposits. Deposit porosity, layers thickness, and depletion of the inhibitor by adsorption on deposits could not be linked entirely to corrosivity and inhibitors performance.

KEY WORDS: carbon steel, CO_2 corrosion, corrosion inhibitors, under-deposit corrosion

INTRODUCTION

Several oil and gas systems which operate in CO_2 conditions can contain mineral deposits which are transported throughout pipelines. As a result, it can cause corrosion problems to occur, such as under-deposit corrosion (UDC).[1-2] This phenomenon is usually related to a localized form of attack underneath the deposits which may be present in oil and gas transportation pipelines.[3-4] The variety of different deposit materials that can occur in pipelines makes the mechanism of UDC quite complex. In general, the deposits can be of inorganic and organic nature. Inorganic deposits like sand, scales, and corrosion products and organic like wax, asphaltene, and inhibitor residues.[5] Sometimes complex mixtures of organic and inorganic deposits are formed such as "schmoo" found in production water facilities[6-9] or more adverse combinations like biofilms and minerals deposits leading to UDC-microbiologically influenced corrosion.[10]

Regarding mineral deposits, silica sand (SiO_2) is often the most abundant mineral found in petroleum pipelines in volumetric concentrations from 1% to 40%.[11] SiO_2 is found in the formation and transported through the pipelines. Other inorganic deposits include corrosion products such as iron carbonates, iron sulphides, iron oxides, among others.[12] Scales are also common inorganic deposits which precipitate from produced water like calcium carbonate ($CaCO_3$), calcium sulphate, and barite sulphate (barite).[13]

One of the most common strategies for UDC mitigation is the use of chemical treatment to extend the lifetime of pipelines. Corrosion inhibitors play an essential role in the protection of carbon steel containing settled particles.[14] Inhibitor molecules are absorbed on metal surfaces, developing a protective barrier against corrosion. For instance, cationic-surfactants such as Cetyl pyridinium chloride monohydrate (CPC) and 1-Dodecyl pyridinium chloride hydrate (DPC) have been investigated to prevent UDC. DPC inhibitor particularly decreases corrosion dissolution by adsorbing at the bare metal surface creating a corrosion protective layer.[15] The increase of DPC concentration is known to alter the adsorbed aggregate morphology from hemispherical to cylindrical which lower corrosion rates at carbon steel surfaces.[16] Other groups of UDC inhibitors are the pyrimidine derivatives compounds such as 2-mercaptopyrimidine (MPY) which have been reported as highly effective in preventing corrosion at deposit-covered steel surfaces. MPY is a polar molecule with the S and N atoms being the negative and positive end of the dipole, respectively.[17] Reznik, et al.,[18] suggested that the performance of pyrimidine derivatives is related to the creation of strong surface complexes with the metal, modifying the cathodic and anodic reactions. The inhibition performance involves many factors that determine the ability of inhibitors to pass through the deposit layers. Thus, it is crucial to evaluate both inhibitor and deposit properties. The inhibitors' properties include the mechanism of inhibitor adsorption on steels, solubility in water and hydrocarbon phases, and inhibitors' adsorption on the different type of deposits or mixtures. The properties of a deposit determine the ability of inhibitors to penetrate to the steel surface include surface area, deposit thickness, and surface charge.[19] It is commonly believed that in optimal conditions an appropriate amount of inhibitor could be enough to provide corrosion protection. However, the presence of deposits can affect the efficiency of a corrosion inhibitor by reducing its availability at the steel surface. Indeed, Binks, et al.,[20] pointed out the importance of predicting the parasitic adsorption of inhibitors onto deposits which can lead to a decrease in inhibitor performance on the underlying metal surface.

Submitted for publication: April 1, 2019. Revised and accepted: June 28, 2019. Preprint available online: June 28, 2019, https://doi.org/10.5006/3223.
‡ Corresponding author. E-mail: K.Lepkova@curtin.edu.au.
* Curtin Corrosion Centre (CCC), Western Australia School of Mines: Minerals, Energy and Chemical Engineering (WASM-MECE), Curtin University, Kent St, Bentley, Perth, Western Australia 6102, Australia.

ISSN 0010-9312 (print), 1938-159X (online)

Table 1. *Names, Abbreviation, Formulas, and Concentrations of Corrosion Inhibitors*

Inhibitor	Abbreviation	Chemical Formula	Concentration (mg/L)	Molar Concentration (mM)	CMC (mM)
Cetylpiridinium chloride monohydrate	CPC	$C_{21}H_{38}ClN \cdot H_2O$	100	0.279	0.006[(A)]
2-Mercaptopyrimidine 98%	MPY	$C_4H_4N_2S$	100	0.892	NA
1-Dodecylpiridinium chloride hydrate 98%	DPC	$C_{17}H_{30}ClN \cdot xH_2O$	100	0.352	0.211[(A)]

[(A)] CMC: Critical micelle concentration (CMC) determined by the pendant drop method. These results compare favorably to CMCs for CPC and DPC of 0.006 mM, and 0.211 mM, respectively, reported elsewhere.[16-17]

Table 2. *Properties of the Evaluated Deposits*

Deposit	Linear Formula	Supplier	Grain Size (μm)[(A)]	Bulk Density (g/cm^3)[(B)]	Porosity (%)[(C)]	Thickness (mm)[(D)]
Silica sand	SiO_2	Sigma-Aldrich	300	1.45	27	8
Aluminum oxide	Al_2O_3	Sigma-Aldrich	24	0.89	67	13
Calcium carbonate (light)	$CaCO_3$	Chem-supply	3	0.32	80	25

[(A)] Grain size determined elsewhere.[17]
[(B)] Bulk density: the mass of deposit particles divided by the volume they occupy.
[(C)] Porosity: volume of the pores or interstices of the deposit, to the total volume of the mass.
[(D)] Thickness of 8 g of deposit above the steel and placed it into a holder.

Previous studies conducted by Pandarinathan, et al.,[17] evaluated the effect of silica sand on the performance of MPY and DPC on carbon steel surfaces. In the present study, the work has been extended to determine if the presence of Al_2O_3 and $CaCO_3$ can affect corrosion inhibitor efficiency on carbon steel surfaces under a CO_2 environment. The adsorption properties of CPC were also evaluated, but this inhibitor was excluded from further corrosion tests due to its strong adsorption on the deposit materials. UV spectroscopy was used to measure inhibitor adsorption onto these materials. This technique has been proven in previous studies as a simple but robust tool to determine inhibitor residuals after adsorption on minerals.[17,21] In this work, results from adsorption test were linked to corrosion inhibition efficiency assessed by potentiodynamic polarization measurements. This research aimed to gain insight into the understanding of inhibitors performance on carbon steel surfaces covered with deposits of different properties, such as mineral type, surface charge, porosity, and particle size.

EXPERIMENTAL

2.1 | Test Materials

The inhibited solutions were prepared in a brine that consisted of 3% sodium chloride NaCl (Chem-supply[†] analytical grade, 99.9%) and 0.01% sodium hydrogen carbonate $NaHCO_3$ (Chem-supply[†], analytical grade 99.7%). These salts were dissolved in ultra-pure water Milli-Q[†] system with resistivity 18.2 MΩ·cm. Subsequently, the brine was saturated with dissolved CO_2 by sparging for 2 h and adding a corrosion inhibitor. Corrosion inhibitors were supplied from Sigma-Aldrich[†]; their information is displayed in Table 1. The properties and general information of the deposits tested are shown in Table 2. The particle size porosity and bulk density of each deposit were measured elsewhere.[12,22] The chemical composition of the carbon steel (1030) used for the tests is as follows (wt%): C (0.37%), Mn (0.80%), Si (0.282%), P (0.012%), S (0.001%), Cr (0.089%), Ni (0.012%), Mo (0.004%), Sn (0.004%), Al (0.01%), and Fe (balance).

[†] Trade name.

2.2 | UV-Spectrophotometry

UV-spectrophotometry was used to evaluate the adsorption of corrosion inhibitors on deposits. Initially, a calibration curve was created using inhibited solutions over a concentration range of 10 ppm through 200 ppm. The correlation coefficient (R^2) values were as a follows 0.9999, 0.9934, and 0.9998 for MPY, DPC, and CPC, respectively, showing an acceptable calibration. Inhibitor adsorption was performed by mixing 8 g of a mineral with 100 mL of inhibited test solutions (100 mg/L) in glass bottles. The bottles were then sparged with CO_2 for 2 h, capped and kept at 30°C with stirring for 24 h or 48 h to allow inhibitor adsorption to occur. Stirring and temperature were achieved using a Ratek[†] orbital shaker-incubator at 150 rpm. After each adsorption period, the total content was centrifuged twice at 3260× g for 40 min to remove mineral particles from the solution before UV analysis. The pH of the inhibited solutions was measured before and, after deposits addition (for each adsorption period). The absorbances were recorded at a wavelength range of 230 nm through 300 nm using a JASCO V-670 UV-Vis[†] spectrophotometer. The amount of corrosion inhibitor adsorbed after each adsorption time was determined from the calibration curve. The reduction of inhibitor concentration corresponded to the amount of inhibitor adsorbed in mg/g (q_{ads}) on the mineral and was calculated using the following equation:[23]

$$q_{ads} = \frac{(Ci - Cf) \times V}{M} \quad (1)$$

where C_i corresponds to the inhibitor concentration before deposit addition in mg/L = 100 mg/L, C_f is the final inhibitor concentration in the solution after contact with deposits, V is the volume of the test solution in liters = 0.1 L, and M is the mass of the deposits in grams = 8 g.

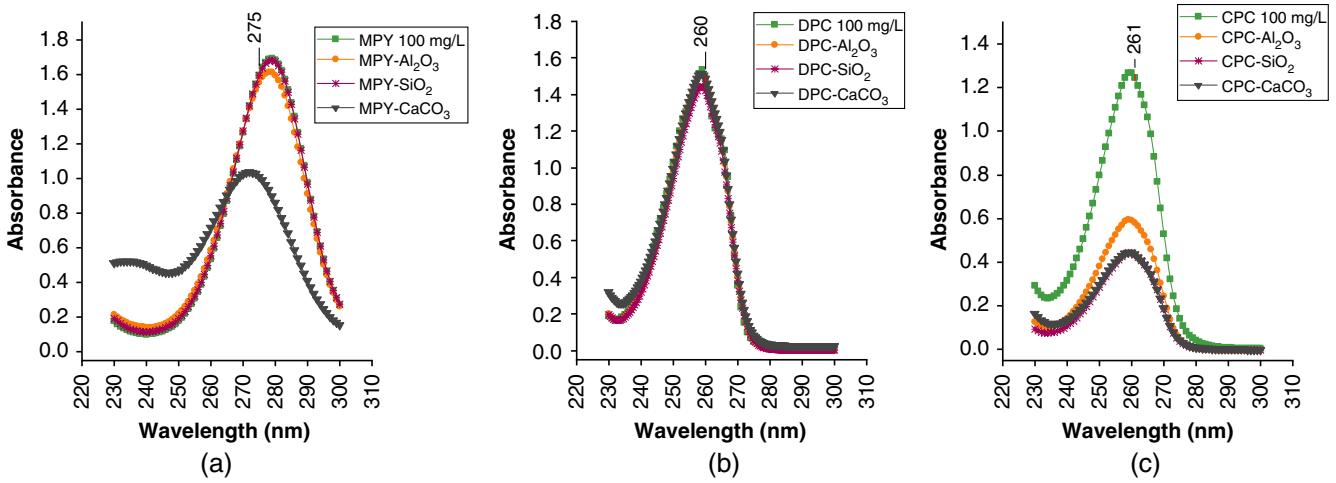

FIGURE 1. *UV absorbance spectra of inhibited solutions after 48 h adsorption period on mineral deposits at 30°C in a CO_2 environment. Each set of the test includes the spectrum for the inhibited solutions (without deposit present) at 100 mg/L.*

The CMC of the surfactant corrosion inhibitors CPC and DPC was determined by the pendant drop method using KSV CAM 200 goniometer and is included in Table 1.

2.3 | Electrochemical Measurements

Carbon steel samples were prepared as working electrodes by electro-coating with Powercron 6000cx† and embedding in epoxy resin (Epofix†), leaving 0.785 cm^2 of the steel surface exposed. Subsequently, the surface area was ground to 1200 grit finish (SiC paper), washed with ethanol and dried with N_2. The sample mounted in the resin was coupled with a holder which was filled with 8 g of each deposit and, thus covering the entire sample surface with a uniform deposit layer. The reference electrode was a single junction Ag/AgCl electrode placed into a capillary with a porous ceramic tip (filled with 3 M KCl), and a 3.5-mm diameter rod of Hastelloy C† was used as a counter electrode. The capillary and the tip of the capillary was placed in close proximity to the steel surface within the deposit layer in order to minimize errors due to IR drop.[17] The assembled electrochemical cells were deoxygenated using N_2 gas for 15 min before contact with the solution. The inhibited solutions containing 100 mg/L of each inhibitor were sparged with CO_2 for 2 h. Then, dissolved oxygen was measured to ensure <20 ppb oxygen in the inhibited solutions before their transfer into the test cell. Afterward, 100 mL of the solution was pumped into the deaerated cell, using a low gas permeability TYGON®† tubing. The test temperature was set at 30°C using an IKA RTC† digital hotplate under thermocouple control and, the CO_2 flow was maintained for the total immersion period.

Electrochemical measurements were performed using a Gamry Reference 600† potentiostat (Gamry Instruments, Inc.). Ten linear polarization resistance (LPR) measurements were recorded within the 24 h of immersion period. The LPR measurements were performed using a potential perturbation of ±10 mV_{OCP} and a scan rate of 0.1667 mV/s with an initial potential of −10 mV. The corrosion rates from LPR measurements were calculated assuming the Stern-Geary constant of 26 mV.[24] Potentiodynamic curves were recorded after 24 h of immersion and LPR measurements had been completed. They were performed with an initial potential of −0.25 V scanning through to + 0.25 V_{OCP} at a scan rate of 0.1667 mV/s.

A total of 12 electrochemical tests, that included the LPR measurements followed by potentiodynamic scans, were performed to investigate UDC and the performance of MPY and DPC corrosion inhibitors. Tests conditions were as follows: (1) a blank, bare steel in un-inhibited test solution; (2) SiO_2, Al_2O_3, and $CaCO_3$ deposit-covered steel in uninhibited test solution; (3) bare steel in MPY and DPC inhibitor test solutions; and (4) SiO_2, Al_2O_3, and $CaCO_3$ deposit-covered steel in MPY and DPC test solutions. During the test period, the solutions were continuously sparged with CO_2 gas.

RESULTS AND DISCUSSION

3.1 | Inhibitors Adsorption on Mineral Deposits by UV-Spectrophotometry

Figures 1(a), (b), and (c) display the UV spectra of inhibited solutions, MPY, DPC, and CPC, respectively, after 48 h adsorption on Al_2O_3, SiO_2, and $CaCO_3$ mineral deposits. Spectra of each inhibitor solution (100 mg/L), without the deposit, is also included in these figures. The wavelength of maximum adsorption for the inhibitors was MPY 275 nm, DPC 260 nm, and CPC 261 nm. Table 3 shows the amount of inhibitor absorbed (q_{ads}), as a function of contact time (24 h and 48 h), for each mineral, obtained from UV absorbance intensities, measured at the maximum absorbance wavelength (λ_{max}). Figure 2 shows the final inhibitors concentrations after contact with deposits. DPC results revealed minimal adsorption of this inhibitor on all deposits. After 48 h of the contact period, DPC concentration in the presence of Al_2O_3 and $CaCO_3$ was 97.41 mg/L and 97.66 mg/L, respectively.

The concentration of MPY only slightly decreased in the presence of SiO_2 and Al_2O_3. However, in the presence of $CaCO_3$, the inhibitor concentration was significantly reduced resulting in 60.07 mg/L at 24 h and 59.25 mg/L at 48 h contact periods. These results indicate that the MPY inhibitor has a high affinity for the $CaCO_3$ deposit reducing its amount considerably in the solution. A possible explanation for this high adsorption of MPY on $CaCO_3$ is that MPY is oppositely charged compared to $CaCO_3$. Pandarinathan, et al.,[17] stated that MPY had a strong electronegative sulphur atom (absorption center) which had less attraction to surfaces charged negatively like silica sand. Calcium carbonate surface, on the other hand, carries a stable positive charge in this acidic environment.[25] It is worth mentioning that the spectrum of MPY inhibitor with $CaCO_3$ deposit had a slight

Table 3. *Adsorption of Corrosion Inhibitors on Mineral Deposits After 24 h and 48 h Assessed by UV-Visible Spectrophotometry*[A]

Initial Inhibitor Concentration (C_i) (mg/L)	Exposure Time (h)	pH	Absorbance (λ_{max})	Inhibitor Absorbed (q_{ads}) (mg/g)[B]	Percentage Adsorption (%)
CPC 100 ppm (λ_{max} 1.27) pH: 4.78	Al_2O_3-24 h	4.85	0.60	0.66	53.0
	Al_2O_3-48 h	4.84	0.59	0.67	53.5
	$CaCO_3$-24 h	6.52	0.41	0.85	68.3
	$CaCO_3$-48 h	6.45	0.41	0.85	68.3
	SiO_2-24 h	4.92	0.48	0.78	62.6
	SiO2-48 h	4.95	0.44	0.82	65.4
DPC 100 ppm (λ_{max} 1.69) pH: 4.81	Al_2O_3-24 h	4.93	1.53	0.01	0.8
	Al_2O_3-48 h	4.99	1.51	0.03	2.6
	$CaCO_3$-24 h	6.79	1.53	0.02	1.3
	$CaCO_3$-48 h	6.19	1.51	0.03	2.3
	SiO_2-24 h	4.84	1.49	0.05	3.6
	SiO2-48 h	4.87	1.45	0.09	6.9
MPY 100 ppm (λ_{max} 1.69) pH: 4.77	Al_2O_3-24 h	4.91	1.65	0.08	6.7
	Al_2O_3-48 h	4.86	1.65	0.08	6.8
	$CaCO_3$-24 h	6.14	1.07	0.50	39.9
	$CaCO_3$-48 h	6.26	1.05	0.51	40.7
	SiO_2-24 h	4.91	1.69	0.06	4.5
	SiO2-48 h	4.86	1.66	0.07	6.0

[A] The table also includes pH values of the inhibited solutions before and after 24 h and 48 h contact with deposits.
[B] q_{ads} amount of inhibitor absorbed in mg/g of mineral.
Equation: (C_i-C_f) x V/M Ci initial inhibitor concentration,
C_f final inhibitor concentration = volume of solution in L,
M = mass of mineral.

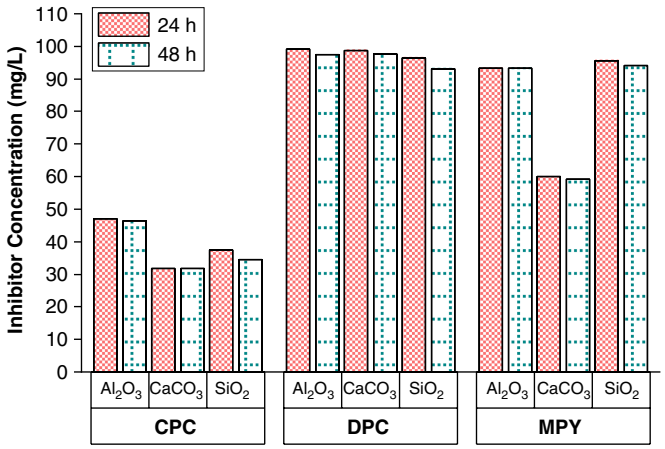

FIGURE 2. *Final inhibitors concentration after 24 h and 48 h adsorption period on mineral deposits at 30°C in a CO_2 environment. The initial concentration of the inhibited solution (100 mg/L).*

shift in wavelength (Figure 1[a]). A possible explanation for this shift is that the supernatant in the inhibited solution remained slightly turbid after contact with $CaCO_3$. This observation suggests that there was an incomplete separation of the mineral from the test solution even after the high-speed centrifugation.

CPC was the inhibitor which was most adsorbed onto all of the deposits at both contact times. Whereas the other surfactant molecule, DPC was not significantly adsorbed. The reason for the different adsorption could be related to the difference in the alkyl chain length between the DPC (C_{12}) and CPC (C_{16}). The length of the alkyl chain has a significant influence on their critical micelle concentration (CMC). The CMC for CPC is about thirty times less than DPC in the test solution used in this investigation. This means there would be an appreciably greater number of CPC micelles compared to DPC micelles in solution. It is generally recognized that micelles or agglomerated molecules are more easily adsorbed on to solid materials than single molecules. It is postulated that the greater adsorption of CPC is due to the larger number of micelles present and their greater affinity to adsorb to mineral surfaces. CPC was not investigated for preventing UDC because of its strong adsorbance to the mineral deposits and similar chemical molecular properties to DPC. This inhibitor also has shown poor performance on sand deposit-covered carbon steel recording corrosion rate of 0.43 mm/y after 72 h contact with this cationic surfactant.[17] Therefore, the authors selected the best performing inhibitors compounds for further evaluation in the presence of different deposits.

Regarding the effect of pH in the bulk solution, it is known to be an important influential parameter in the corrosion process of bare carbon steel surfaces under CO_2 conditions.[26-27] However, previous studies demonstrated that the bulk solution pH did not affect the CO_2 corrosion of mild steel in the presence of mineral deposits. The authors also founded higher surface pH values beneath the silica sand, SiO_2 powder and glass beads than the bulk solution suggesting different water chemistry within

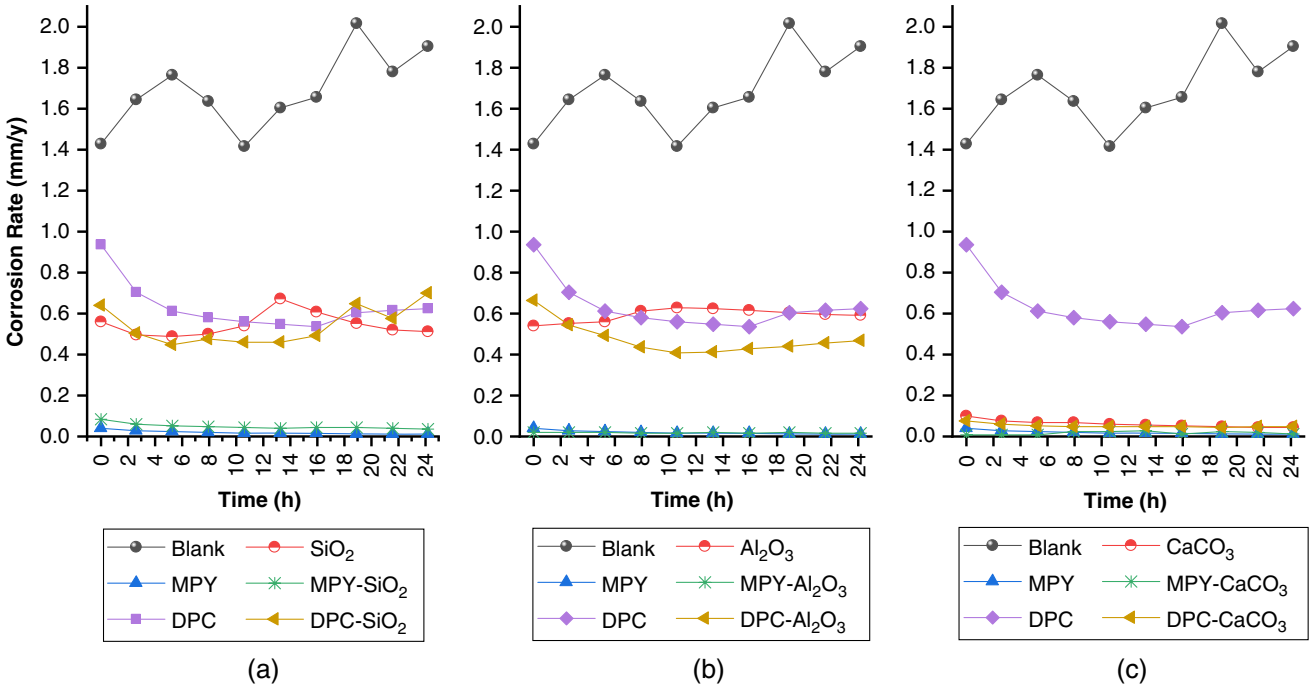

FIGURE 3. *Corrosion rates of deposit-covered carbon steel surfaces determined by LPR measurements during 24 h immersion in CO_2-inhibited and uninhibited solutions. Deposits: silica sand (SiO_2), aluminum oxide (Al_2O_3), and calcium carbonate ($CaCO_3$). Blank is a specimen of bare or nondeposited steel in uninhibited test solution (3% NaCl, 0.01% $NaHCO_3$, saturated with CO_2).*

or underneath the deposit layers.[22] Although, in the present study, the pH of the inhibited test solutions in contact with $CaCO_3$ had a higher pH >6 when compared to the pH values <5 in the presence of SiO_2 and Al_2O_3 (Table 3). It is not possible to infer that the pH in bulk could directly affect the corrosion process in the underlying steel surfaces covered with these mineral deposits.

3.2 | Corrosion Monitoring by Linear Polarization Resistance Measurements

Figure 3 shows corrosion rates monitored over 10 LPR measurements taking during 24 h immersion for all of the 12 experimental conditions. Figure 3(a) gives the results for (1) the blank or bare steel in an uninhibited test solution, (2) DPC and bare steel, (3) MPY and bare steel, (4) SiO_2 deposit-covered steel, (5) MPY and SiO_2 deposit-covered steel, and (6) DPC and SiO_2 deposit-covered steel. Figure 3(b) shows the results for (1) the blank or bare steel in an uninhibited test solution, (2) DPC and bare steel, (3) MPY and bare steel, (4) Al_2O_3 deposit-covered steel, (5) MPY and Al_2O_3 deposit-covered steel, and (6) DPC and Al_2O_3 deposit covered steel. Figure 3(c) shows the results for (1) the blank or bare steel in an uninhibited test solution, (2) DPC and bare steel, (3) MPY and bare steel, (4) $CaCO_3$ deposit covered steel, (5) MPY and $CaCO_3$ deposit-covered steel, and (6) DPC and $CaCO_3$ deposit-covered steel.

In general, the corrosion rates remained reasonably constant throughout the experimental period (24 h) except for the DPC test without a deposit. The first LPR measurement (1 h immersion) recorded a corrosion rate of 0.94 mm/y and the last measurement (24 h) a corrosion rate of 0.62 mm/y. This indicates that a minimum of 6 h contact of DPC is needed to protect the bare steel against corrosion. It is also a good indication of the low rate at which this cationic surfactant adsorbs onto bare steel surfaces to form an assembled protective film. The reduction of the uninhibited corrosion rate from 1.5 mm/y to 2 mm/y for the blank solution to 0.62 mm/y in the presence of DPC demonstrates the relatively poor performance of DPC as a corrosion inhibitor.

DPC did not demonstrate good performance in preventing UDC at Al_2O_3 (Figure 3[b]) and SiO_2 (Figure 3[a]) deposit-covered surfaces. Under these deposits, DPC solutions achieved maximum inhibition after 6 h immersion, followed by a steady-state inhibition period until approximately the 16th hour. Afterward, the corrosion rates increased reaching values of 0.47 mm/y for Al_2O_3 and 0.70 mm/y for SiO_2 after 24 h of immersion. The $CaCO_3$-deposit-covered steel surface recorded the least corrosion rates <0.1 mm/y in DPC-test solution.

In contrast, MPY was shown to be highly efficient on the bare surface with corrosion rate values below 0.04 mm/y during the immersion period. MPY was also very effective in reducing UDC as can be seen in Figures 3(a) through (c) where the corrosion rates for all of the deposits was below 0.05 mm/y after 6 h. At 24 h the corrosion rates reached 0.037 mm/y, 0.015 mm/y, and 0.012 mm/y, respectively, under SiO_2, Al_2O_3, and $CaCO_3$ deposits demonstrating the superior performance of this heterocyclic molecule.

Concerning the effect of the deposits on carbon steel corrosion, it can be seen that all deposit-covered steel surfaces, in the absence of inhibitor, had lower corrosion rates when compared with the bare steel (Figures 3[a] through [c]). Al_2O_3 had the highest average corrosion rates (0.59 mm/y) Figure 3(b) followed very close by SiO_2 (0.51 mm/y) Figure 3(a). The least corrosive was $CaCO_3$ deposit with corrosion rates values <0.1 mm/y Figure 3(c).

3.3 | Potentiodynamic Polarization Measurements (Tafel Plots)

As mentioned earlier, only DPC and MPY inhibitors were selected for electrochemical measurements due to their low adsorption on most mineral deposits (inhibitors adsorption

results). Figures 4(a) through (f) display the potentiodynamic curves recorded after 24 h of immersion for each experimental condition described in the Experimental section (Electrochemical Measurements). The diagrams in the figures are arranged as follows: Figures 4(a), (c), and (e) show the performance of MPY in the presence and absence of SiO_2, Al_2O_3, and $CaCO_3$ deposits. Figures 4(b), (d), and (f) give corresponding potentiodynamic curves for DPC. Curves for SiO_2, Al_2O_3, and $CaCO_3$ deposits without inhibitor present are also provided in respective, applicable figures. The blank curve recorded for bare steel exposed in the uninhibited test solution (CO_2 saturated 3% NaCl, 0.01% $NaHCO_3$) is also provided in each figure. This enables the relevant effect of the inhibitor and the deposit on the corrosion process to be observed or compared. Table 4 shows the

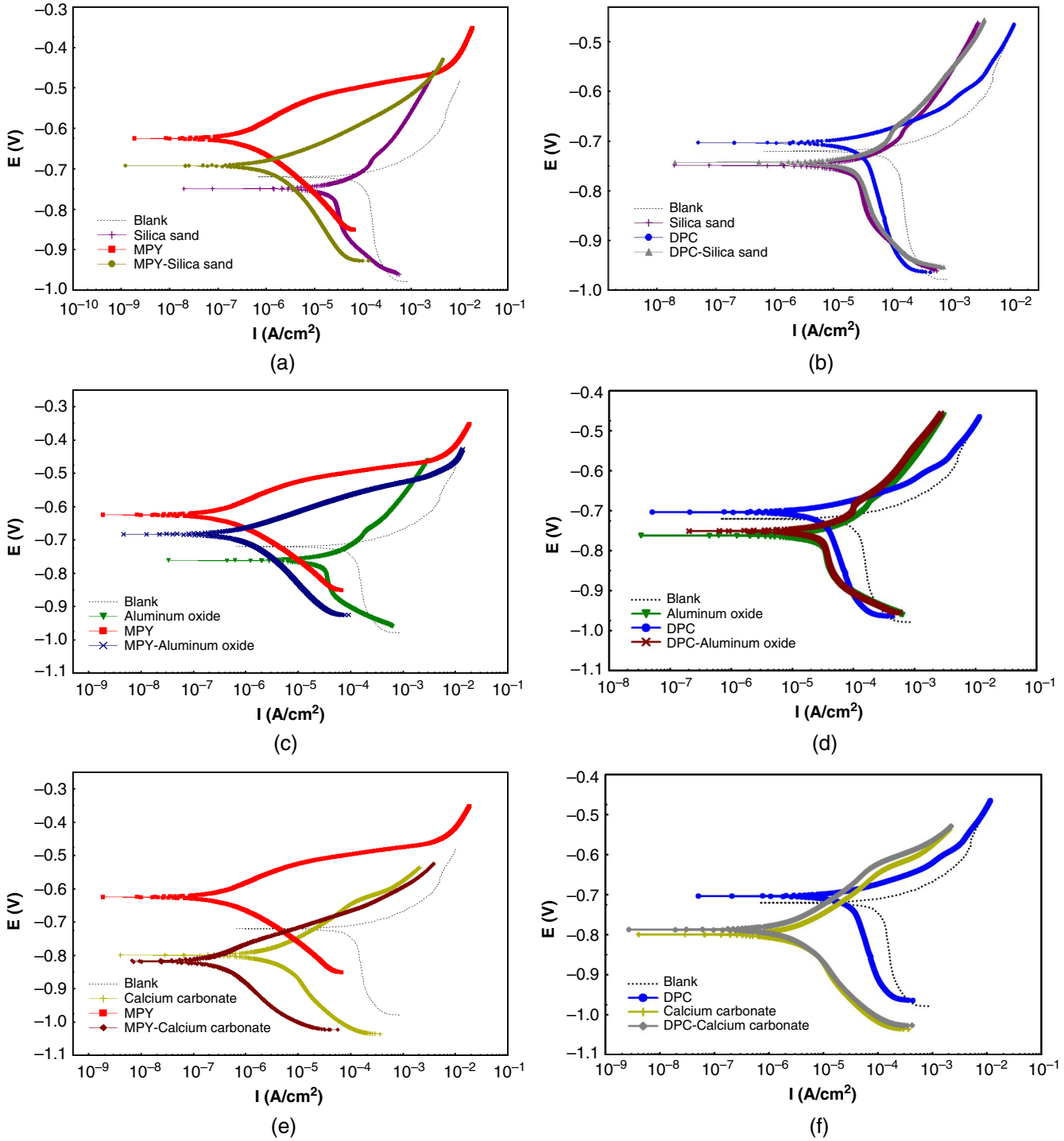

FIGURE 4. *Potentiodynamic polarization curves recorded at bare and deposit-covered-steel surfaces in uninhibited and inhibited solutions (100 mg/L) at 30°C after 24 h immersion period under CO_2 environment. Combinations of (a) silica sand and MPY, (b) silica sand and DPC, (c) aluminum oxide and MPY, (d) aluminum oxide and DPC, (e) calcium carbonate and MPY, and (f) calcium carbonate and DPC. In each figure, a blank, the potentiodynamic curve recorded for bare steel exposed in uninhibited test solution has been included for a comparative purpose.*

Table 4. *Electrochemical Parameters of the Carbon Steel Derivated from Potentiodynamic Polarization Measurements in Figure 4*

Test	βa (V/dec)	−βc (V/dec)	E_{corr} ($V_{Ag/AgCl}$)	i_{corr} (μA/cm^2)	v_{corr} (mm/y)
Blank[(A)]	0.08	0.92	−0.73	122.53	1.42
SiO_2	0.11	0.47	−0.75	24.68	0.29
Al_2O_3	0.12	0.50	−0.77	28.98	0.34
$CaCO_3$	0.10	0.18	−0.79	3.41	0.04
MPY	0.06	0.07	−0.62	0.22	<0.01
MPY-SiO_2	0.05	0.12	−0.69	1.23	0.01
MPY-Al_2O_3	0.05	0.09	−0.68	0.51	<0.01
MPY-$CaCO_3$	0.06	0.14	−0.81	0.32	<0.01
DPC	0.05	0.41	−0.70	31.25	0.36
DPC-SiO_2	0.11	0.32	−0.75	23.72	0.28
DPC-Al_2O_3	0.12	0.44	−0.76	27.92	0.32
DPC-$CaCO_3$	0.09	0.14	−0.78	2.10	0.02

[(A)] Blank is bare steel electrode exposed to the uninhibited test solution.

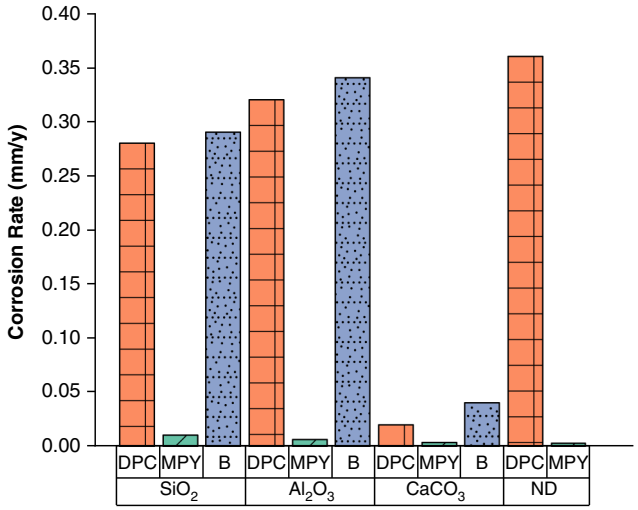

FIGURE 5. *Corrosion rates calculated from potentiodynamic measurements after 24 h of immersion period. B: deposit-covered steel in uninhibited solution. ND: no deposits.*

electrochemical parameters, such as corrosion potential (E_{corr}), corrosion current density (i_{corr}), and Tafel constants (βa, βc) obtained from the potentiodynamic polarization measurements.

3.4 | Effect of Deposits on Corrosion of Carbon Steel (Tests in Uninhibited Solutions)

It can be seen in Figures 4(a), (c), and (e), Table 4 and Figure 5 that the deposits had a favorable effect on reducing i_{corr} and the average corrosion rate. Compared to the blank or undeposited or bare steel, the corrosion rate was reduced from 1.42 mm/y to 0.29 mm/y, 0.34 mm/y, and 0.04 mm/y in the presence of SiO_2, Al_2O_3, and $CaCO_3$, respectively (Table 4). The deposits also shifted the corrosion potential to more negative values in the order of −20 mV, −40 mV, and, −60 mV for SiO_2, Al_2O_3, and $CaCO_3$, respectively. Generally speaking the overall shapes of the anodic and cathodic curves for SiO_2 and Al_2O_3 deposit-covered steel remained similar to the blank. In the case of $CaCO_3$, there was a more noticeable change in the shape of the cathodic curve (Figure 4[e]) and reduction in corrosion rate (Figure 4[e] and Table 4). This can be attributed to the alkaline nature of the $CaCO_3$ resulting in an increase in pH at the surface and the electrolyte in the pores of this deposit resulting in a dramatic reduction in the average corrosion rate to 0.04 mm/y. The surface pH and the electrolyte in the pores of the $CaCO_3$ deposit would be higher than the bulk solution (pH 6.65) which was buffered by the continual sparge of CO_2 gas. These results are in general agreement with the deposits having a blocking effect in reducing the rate of mass transfer of corroding species (H_2CO_3 and H^+) to the steel surface. This reduction in mass transfer can also cause the interfacial pH to increase resulting in a negative shift in the corrosion potential and reduction in corrosion rate. Huang, et al.,[22] and Pandarinathan, et al.,[12] stated that inert deposits provide a barrier to the mass transfer of corrosive species and a reduction in average corrosion rates. The cathodic and anodic curves recorded for bare steel in Figure 4 are typical for CO_2 corrosion of steel. In the case of the cathodic reaction, the reaction goes from kinetic or charge transfer control to mixed control and mass transfer control as the polarization increases negatively from the corrosion potential. It is difficult to obtain a Tafel slope measurement as there is no extended Tafel region. Nevertheless, the β_c values given in Table 4 provide a guide to the macroscopic changes in Tafel behavior. Drawing a comparison between oxygen and CO_2 corrosion is interesting. In the case of oxygen corrosion, the area under a deposit (deoxygenated region) behaves as the anode while the area outside of the deposit (oxygen-rich region) behaves as the cathode. CO_2 corrosion of steel has the opposite effect, at least early in the corrosion process. The areas under the deposit behave as the cathode (shifted to a more negative potential) while areas of bare steel outside the deposit undergoes a greater rate of corrosion. It is, however, emphasized, that with time, localized anodes and cathodes can develop under deposits resulting in pitting or localized forms of corrosion.

In relation to the corrosive behavior under each deposit, values given in Table 4 and Table 5 indicate that Al_2O_3 produced

the highest average corrosion rate of 0.34 mm/y followed by SiO_2 with 0.29 mm/y and $CaCO_3$ with only 0.04 mm/y. These corrosion rates are lower than those obtained from LPR measurements, namely 0.59 mm/y for Al_2O_3, 0.51 mm/y for SiO_2 and <0.1 mm/y for $CaCO_3$. The difference is probably due to errors incurred extrapolating the Tafel region back to the corrosion potential. The corrosiveness of Al_2O_3 deposit under CO_2 ambience has been previously associated with a low pH developing underneath of the deposit as a result of its hydrolysis.[12] Huang, et al.,[22] on the other hand, correlated high deposit porosity with high corrosion rates. In the present study, porosities of Al_2O_3 (67%) and, SiO_2 (27%) cannot be associated with an order of corrosivity as $CaCO_3$ had the highest porosity (80%) and yet it was the least corrosive. As discussed earlier, the most likely reason for the low corrosion rates measured in the presence of calcium carbonate (Table 4) is the alkaline nature of this mineral. Naturally, calcium carbonate precipitates in the crystalline forms of calcite, aragonite, vaterite, calcium carbonate monohydrate, and calcium carbonate hexahydrate. However, calcite is the only thermodynamically stable form under normal conditions.[28] Patra, et al.,[25] stated that the surface Ca^{2+} and CO_3^- ions could undergo hydrolysis in acidic solutions making the mineral more positive and the solution more alkaline. The pH of calcite is approximately 9.9, and it and other crystalline forms of $CaCO_3$ would, therefore, increase the pH at the steel surface. In the presence of CO_2 the solubility of $CaCO_3$ can increase due to the formation of more soluble calcium bicarbonate by the following reaction:

$$CaCO_3 + H_2O + CO_2 \rightarrow Ca(HCO_3)_2 \rightarrow Ca^{2+} + 2HCO_3^- \quad (2)$$

The overall effect would be for the carbonate and bicarbonate to increase pH at the steel surface.

3.5 | Corrosion Inhibitors Performance on Bare and Deposit-Covered Steel Surfaces (Tests with Inhibited Solutions)

It is acknowledged that there are several testing methods to evaluate inhibitors performance in the presence of deposits. Each model differs in the design and thus, assess this UDC phenomenon and its mitigation in different ways.[29] For instance, multielectrode arrays systems have been used the study inhibitor efficiency at the bare and deposit-covered steel surfaces allowing to visualize electrochemical differences beneath and outside the deposit[30] or in precorroded systems.[31] In this study, however, the inhibition performance was evaluated at carbon steel surfaces completely covered with a sand deposit. Previous studies have used this configuration to evaluate UDC inhibition, where it was founded electrochemical differences compared to bare steel surfaces.[17] It can be seen in Table 4 that the inhibitors, when there was no deposit present, caused the corrosion potential to shift positively. This was particularly noticeable with MPY where the corrosion potential changed from −0.73 V to −0.62 V or +110 mV (Table 4). The shift in corrosion potential with DPC was less positive, i.e., from −0.73 mV to −0.70 mV or +30 mV.

In the presence of silica sand and aluminum oxide, MPY still caused the corrosion potential to shift positively. However, this was not the case with calcium carbonate where the potential was negative relative to the corrosion potential of bare steel in uninhibited solution. With DPC the corrosion potential was negative relative to the blank in all cases when there was deposit present.

As discussed in the Section Effect of Deposits on Corrosion of Carbon Steel (Tests in Uninhibited Solutions), the mass transfer limited region of the cathodic curve for CO_2 corrosion of steel (blank Figures 4[a] through [f]) is classical of CO_2 corrosion of carbon steel. In the presence of MPY, the corrosion process became more kinetically or charge transfer controlled. This can be seen in Figures 4(a), (c), and (e), whereby comparison to the blank, the mass transfer region of the cathodic curve has disappeared to demonstrate greater Tafel behavior or a better linear relationship between the logarithm of current and voltage. The influence of DPC on the cathodic curve for CO_2 corrosion, however, was not marked. In the presence of SiO_2 and Al_2O_3 deposits, the mass transfer cathodic region was still evident. However, as outlined in Table 4, it was a slight decrease in βc values from 0.41 V/dec in the DPC test to 0.32 V/dec in DPC-SiO_2 test. Similarly, a small change was observed in the presence of Al_2O_3 deposit where the βc values increase from 0.41 V/dec in DPC test to 0.44 V/dec in DPC-Al_2O_3 test. Calcium carbonate, due to its alkaline nature reflected in the bulk pH 6.79 (Table 3), affected the kinetics of both the anodic and cathodic reactions as can be observed in Figures 4(e) and (f) with the changes in Tafel slopes.

All tests with MPY present exhibited the lowest corrosion rate of ≤0.01 mm/y (Table 4) indicating that this inhibitor provides the highest corrosion protection at bare and deposit-covered carbon steel. It can be seen in Figures 4(a), (c), and (e) and Table 4 that at surfaces covered with SiO_2 and Al_2O_3, the addition of MPY shifted the corrosion potential more positively by +40 mV and +0.50 mV respectively compared to the blank. For $CaCO_3$, on the other hand, the potentials shifted more negatively by −0.80 mV compared to the blank. With MPY the overall shape of the anodic and cathodic polarization curves for bare steel remained the same in the presence of a deposit (Figures 4[a], [c], and [e]). This indicates that MPY can penetrate the deposit and influence the surface of the steel similarly to when no material was present.

On the contrary, DPC had little influence on the overall shape of the anodic and cathodic curves compared to the blank and those recorded in the presence of SiO_2 and Al_2O_3 deposits (Figures 4[b] and [d]). $CaCO_3$ however, due to its alkalinity had a marked effect on the shape of the anodic and cathodic curves (Figure 4[f]). As mentioned earlier, DPC caused the corrosion potential of bare steel (blank) to shift positively by only 30 mV (Table 4). The influence of the deposits on the corrosion potential was dominant over the inhibitor. In the presence of DPC, SiO_2 shifted the corrosion potential negative by −20 mV, Al_2O_3 by −30 mV and $CaCO_3$ by −50 mV (Figures 4[b], [d], and [f] and Table 4). It can be seen in Table 4 that DPC was not effective in reducing the corrosion of bare steel and deposit covered steel surfaces compared to MPY.

3.6 | Correlation Between Inhibitors Adsorption and Corrosion Inhibition Performance

The presence of mineral deposits in a system can affect the corrosion inhibitors effectiveness in different ways. De Reus, et al.,[19] suggested that the inhibitors penetration or diffusion rate of inhibitors to go through deposits layers can be influenced by some features of deposits e.g., porosity, layer thickness, surface area, and nature of the deposit including surface charge of the particles. In addition, the concentration of can be depleted by adsorption on mineral deposits.[20] In this study, the low percentage adsorption of DPC on the deposits shown in

Table 5. *Sequences of Inhibitor Adsorption on Deposits, Deposit Corrosivity and Porosity, and Corrosion Inhibition Efficiency at Carbon Steel Surfaces Under CO_2 Conditions*

Inhibitors Adsorption	**Most Adsorbed → Least Adsorbed**								
	$CPC-CaCO_3$	$CPC-SiO_2$	$CPC-Al_2O_3$	$MPY-CaCO_3$	$MPY-Al_2O_3$	$DPC-SiO_2$	$MPY-SiO_2$	$DPC-CaCO_3$	$DPC-Al_2O_3$
Corrosion Inhibition Efficiency	**Highest → Lowest**								
	$MPY-CaCO_3 = MPY-Al_2O_3$			$MPY-SiO_2$	$DPC-CaCO_3$	$DPC-SiO_2$	$DPC-Al_2O_3$		
Deposit Corrosivity	**Highest → Lowest**								
	Al_2O_3	SiO_2	$CaCO_3$						
Deposit Porosity	**Highest → Lowest**								
	$CaCO_3$	Al_2O_3	SiO_2						

Table 3 indicates that these deposits would have little impact on the concentration of DPC. The corrosion rate recorded at the bare surface with DPC was 0.36 mm/y compared to the surfaces covered SiO_2, Al_2O_3, and $CaCO_3$ with values of 0.28 mm/y, 0.32 mm/y, and 0.02 mm/y respectively. That is, in the case of silica and aluminum oxide deposits the corrosion rates were not significantly different from bare steel. In the case of calcium carbonate, the significant reduction in corrosion rate is due to the nature and inherent inhibitor properties of this material. According to these results, the depletion of DPC by absorption on to the deposits was not the critical reason for its relatively poor performance in preventing UDC.

In contrast, MPY provided superior inhibition efficacy in all tests (≤0.01 mm/y). In the test with $CaCO_3$, due to the alkaline nature of this material, the uninhibited corrosion rate was particularly low, i.e., 0.04 mm/y (Table 4). However, MPY was still able to lower the corrosion rate significantly to <0.01 mm/y, despite it being appreciably adsorbed (40.7% depletion) by $CaCO_3$. Results from this work indicate that MPY is as a good candidate for UDC mitigation despite the depletion that can occur in the presence of $CaCO_3$. However, it is worth pointing out that in terms of average corrosion rates, $CaCO_3$ was proven essentially no corrosive in this investigation. Reznik, et al.,[18] demonstrated high inhibition activity of pyrimidine compounds like MPY even in low concentrations (0.02 mg/L to 5 mg/L) suggesting that the efficiency is most probably connected with the chemisorption of inhibitor not on the whole surface but only on active centers. Evidently, the remaining MPY was able to effectively penetrate the settled deposit layers protecting the underlying steel surfaces. Durnie, et al.,[32] mentioned that the affinity of the inhibitor for the deposits and its ability to penetrate the deposit layers are determining parameters for inhibitors performance evaluation. Indeed, the author demonstrated that sulphur species were able to penetrate faster than some quaternary amines and imidazoline compounds. Different factors can influence inhibitors performance, and this includes the presence of deposits. For instance, Pandarinathan, et al., showed that inhibition mechanism of Thiobenzamide changed in the presence of sand deposit.[28] If deposits are present, it is recommended that UDC tests similar to those used in this study are integrated into the test program.

Table 5 summarizes the sequences of adsorption and inhibition performance tests as well as corrosivity of each deposit. Corrosion rates from polarization measurements follow the same order than the ones calculated from LPR measurements (last measurement at approximately 24 h immersion).

CONCLUSIONS

➢ Inhibitor adsorption measurements on Al_2O_3, SiO_2, and $CaCO_3$ mineral deposits using UV spectroscopy revealed that of the two surfactant corrosion inhibitors evaluated, CPC adsorbed substantially greater, from 53% to 68%, on these deposits at the concentration of 100 mg/L tested. On the other hand, DPC adsorbed only 0.8% to 6.9% (Table 3). It is postulated that the greater adsorption of CPC is related to its larger alkyl chain length (C16 as opposed to C12) and lower CMC.

➢ Adsorption of MPY on Al_2O_3 and SiO_2 was only 6.8% and 6.0%, respectively, however, in the presence of $CaCO_3$, it was about 41%. Despite the relatively high percentage adsorption on $CaCO_3$, MPY was shown to be a good inhibitor in preventing UDC with all three mineral deposits investigated. It appears to be a good candidate for preventing this type of corrosion.

➢ In uninhibited solution, the presence of a deposit significantly reduced the baseline corrosion rate measured for bare steel tested under similar conditions, for instance, in the presence of SiO_2, Al_2O_3, and $CaCO_3$ the corrosion rate was reduced from 1.42 mm/y to 0.29 mm/y, 0.34 mm/y, and 0.04 mm/y (Table 4). This reduction in corrosion rate is attributed to the obstruction caused by the deposit and reduction in the mass transfer of corrosive species to the metal surface. The dramatic reduction in corrosion rate caused by $CaCO_3$ (0.04 mm/y) is ascribed to the alkaline nature of this material increasing the pH on the steel surface and, in the bulk from pH ~4.8 to pH >6.1 before and after $CaCO_3$ addition, respectively.

➢ The influence of DPC in reducing the average corrosion rate under deposits was noticeably not much greater than the blockage caused by the deposit itself by diminishing the rate of mass transfer. In the presence of DPC the corrosion rates under, SiO_2, Al_2O_3, and $CaCO_3$ were 0.28 mm/y, 0.32 mm/y, and 0.02 mm/y, respectively. These results can be compared to the aforementioned values of 0.29 mm/y, 0.34 mm/y, and 0.04 mm/y, for deposit-covered steel without inhibitor present (Table 4).

➢ In contrast, MPY substantially reduced the corrosion rate under all of the deposits investigated, for example, in the presence of SiO_2, Al_2O_3, and $CaCO_3$ the corrosion rate was reduced from 0.29 mm/y to 0.01 mm/y, 0.28 mm/y to <0.01 mm/y and 0.04 mm/y to <0.01 mm/y, respectively.

➢ The influence of the deposits on UDC of the steel surface did not appear to be significantly related to their physical properties (Table 2). In the case of $CaCO_3$, the reduction in corrosion rate is most probably related to the chemical properties and alkaline nature of this material.

➢ A test protocol to prevent UDC is worth incorporating into a program to evaluate the effectiveness of inhibitors for controlling

CO_2 corrosion during oil and gas production when sand and deposits are present.

ACKNOWLEDGMENTS

The authors (E. M. S.) would like to thank Curtin University for awarding the Curtin International Postgraduate Research Scholarship (CIPRS).

References

1. T. Esan, S.D. Kapusta, M.J.J. Simon-Thomas, "Case Study: Extreme Corrosion of a 20"-Oil Pipeline in the Niger Delta Region," CORROSION 2001, paper no. 01629 (Houston, TX: NACE, 2001).
2. A. Jenkins, D. MacDougall, "Mitigation of Under-Deposit and Weldment Corrosion with an Environmentally Acceptable Corrosion Inhibitor," CORROSION 2013, paper no. 2508 (Houston, TX: NACE, 2013).
3. Z. Liu, T. Jackson, P. Kearns, "Mechanistic Studies of Sour Underdeposit Corrosion in the Presence of Chemical Inhibition," CORROSION 2015, paper no. 5781 (Houston, TX: NACE, 2015).
4. R. Nelson, M.A. Edwards, P. Kovash, "Monitoring and Controlling Corrosion in an Aging Sour Gas Gathering System a Nine-Year Case History," CORROSION 2007, paper no. 07668 (Houston, TX: NACE, 2007).
5. J. Huang, B. Brown, Y.-S. Choi, S. Nešić, "Prediction of Uniform CO_2 Corrosion of Mild Steel Under Inert Solid Deposits," CORROSION 2011, paper no. 11260 (Houston, TX: NACE, 2011).
6. Y. Zhang, J. Moloney, S. Mancuso, "Understanding Factors Affecting Corrosion Inhibitor Performance in Under-Deposit Testing with Sand," CORROSION 2013, paper no. 2575 (Houston, TX: NACE, 2013).
7. W. Mosher, M. Mosher, T. Lam, Y. Cabrera, A. Oliver, H. Tsaprailis, "Methodology for Accelerated Microbiologically Influenced Corrosion in Under Deposits from Crude Oil Transmission Pipelines," CORROSION 2014, paper no. 4254 (Houston, TX: NACE, 2014).
8. K.T. Ly, D.J. Blumer, W.M. Bohon, A. Chan, "Novel Chemical Dispersant for Removal of Organic/Inorganic Schmoo Scale in Produced Water Injection Systems," CORROSION 1998 (Houston, TX: NACE, 1998).
9. J.R. Vera, D. Daniels, M.H. Achour, "Under Deposit Corrosion (UDC) in the Oil and Gas Industry: A Review of Mechanisms, Testing and Mitigation," CORROSION 2012 (Houston, TX: NACE, 2012), p. 3028-3040.
10. E.M. Suarez, K. Lepková, B. Kinsella, L.L. Machuca, *Int. Biodeteriorat. Biodegrad.* 137 (2019): p. 137-146.
11. Z. Zhenjin, W. Keith, J.T. Patrick, "Solid Deposition in Liquids Petroleum (Oil) and Wet-Gas Pipelines for Internal Corrosion Predictive Modeling (ICPM)," NACE Northern Area Western Conference (Houston, TX: NACE, 2010).
12. V. Pandarinathan, K. Lepková, S.I. Bailey, R. Gubner, "Impact of Mineral Deposits on CO_2 Corrosion of Carbon Steel," CORROSION 2013 (Houston, TX: NACE, 2013).
13. Z. Amjad, K.D. Demadis, *Mineral Scales and Deposits: Scientific and Technological Approaches* (Amsterdam, NL: Elsevier, 2015).
14. S. Papavinasam, *Corrosion Inhibitors* (Hoboken, NJ: John Wiley & Sons, Inc., 2011), p. 1021-1032.
15. K. Lepková, W. Van Bronswijk, V. Pandarinathan, R. Gubner, *Vib. Spectrosc.* 68 (2013): p. 204-211.
16. V. Pandarinathan, K. Lepková, S.I. Bailey, T. Becker, R. Gubner, *Ind. Eng. Chem. Res.* 53, 14 (2014): p. 5858-5865.
17. V. Pandarinathan, K. Lepková, S.I. Bailey, R. Gubner, *Corros. Sci.* 72 (2013): p. 108-117.
18. V.S. Reznik, V.D. Akamsin, Y.P. Khodyrev, R.M. Galiakberov, Y.Y. Efremov, L. Tiwari, *Corros. Sci.* 50, 2 (2008): p. 392-403.
19. H. De Reus, L.J.A. Hendriksen, M. Wilms, Y.N. Al-Habsi, W. Durnie, M. Gough, "Test Methodologies and Field Verification of Corrosion Inhibitors to Address Under Deposit Corrosion in Oil and Gas Production Systems," CORROSION 2005 (Houston, TX: NACE, 2005).
20. B.P. Binks, P.D.I. Fletcher, I.E. Salama, D.I. Horsup, J.A. Moore, *Langmuir: ACS J. Surf. Colloids* 27, 1 (2011): p. 469-473.
21. D. Doležal, T. Bolanca, Š.C. Stefanović, *Materialwiss. Werkst.* 42, 3 (2011): p. 229-233.
22. J. Huang, B. Brown, X. Jiang, B. Kinsella, S. Nešić, "Internal CO_2 Corrosion of Mild Steel Pipelines Under Inert Solid Deposits," CORROSION 2010, paper no. 10379 (Houston, TX: NACE, 2010).
23. C. Blachier, L. Michot, I. Bihannic, O. Barrès, A. Jacquet, M. Mosquet, *J. Colloid Interf. Sci.* 336, 2 (2009): p. 599-606.
24. V. Pandarinathan, K. Lepková, S.I. Bailey, R. Gubner, *J. Electrochem. Soc.* 160, 9 (2013): p. C432-C440.
25. P. Patra, P. Somasundaran, C. Lo, *Impact of Calcium Carbonate Mineral Scales in Industries* (Boca Raton, FL: CRC Press, 2013), p. 309-324.
26. S. Nešić, J. Postlethwaite, S. Olsen, *Corrosion* 52, 4 (1996): p. 280-294.
27. S. Nešić, *Carbon Dioxide Corrosion of Mild Steel* (Hoboken, NJ: John Wiley & Sons, Inc., 2011), p. 229-245.
28. R. Gaur, N. Abbas, *Characterization of Oil-Field Calcium Carbonate Scales* (Boca Raton, FL: CRC Press, 2013), p. 407-422.
29. NACE TG380-24253 "Underdeposit Corrosion (UDC) Testing and Mitigation Methods in the Oil and Gas Industry" NACE International publication 61114 (Houston, TX: NACE, 2014).
30. Y. Tan, Y. Fwu, K. Bhardwaj, *Corros. Sci.* 53, 4 (2011): p. 1254-1261.
31. G. Hinds, A. Turnbull, *Corrosion* 66, 4 (2010): p. 046001-01 to 046010-10.
32. W. Durnie, M. Gough, H. De Reus, "Development of Corrosion Inhibitors to Address Under Deposit Corrosion in Oil and Gas Production Systems," CORROSION 2005 (Houston, TX: NACE, 2005).